Structures of the *Klebsiella aerogenes* Urease Apoenzyme and Two Active-Site Mutants[†,‡]

Evelyn Jabri[§] and P. Andrew Karplus*

Section of Biochemistry, Molecular and Cell Biology, Cornell University, Ithaca, New York 14853

Received February 21, 1996[⊗]

ABSTRACT: Urease from *Klebsiella aerogenes* [Jabri et al. (1995) *Science 268*, 998−1004] is an $(\alpha\beta\gamma)_3$ trimer with each α-subunit having an $(\alpha\beta)_8$-barrel domain containing a binickel active center. Here we examine structure−function relations for urease in more detail through structural analysis of the urease apoenzyme at 2.3 Å resolution and mutants of two key catalytic residues (H219A and H320A) at 2.5 Å resolution. With the exception of the active site, in which a water molecule takes the place of the missing carbamate and nickel atoms, the structure of the apoenzyme is nearly identical to that of the holoenzyme, suggesting a high degree of preorganization which helps explain the tight binding of nickel. In the structure of H219A, the major change involves a conformational shift and ordering of the active site flap, but a small shift in the side chain of $Asp^{\alpha 221}$ could contribute to the lower activity of H219A. In the H320A structure, the catalytic water, primarily a Ni-2 ligand in the holoenzyme, shifts into a bridging position. This shift shows that the nickel ligation is rather sensitive to the environment and the change in ligation may contribute to the 10^5-fold lower activity of H320A. In addition, these results show that urease is resilient to the loss of nickel ions and mutations. Analysis of the urease tertiary/quaternary structure suggests that the stability of this enzyme may be largely due to its burial of an unusually large fraction of its residues: 50% in the γ-subunit, 30% in the β-subunit, and 60% in the α-subunit.

Nickel-dependent ureases have been isolated from a wide variety of bacteria, fungi, and higher plants (Hausinger, 1993). Among the nickel metalloenzymes, which also include hydrogenase, methyl-coenzyme M reductase, and carbon monoxide dehydrogenase, urease is the only one that catalyzes a hydrolysis rather than a redox reaction. The primary physiological role of urease is to allow the organism to use externally and internally generated urea as a nitrogen source [for reviews see Mobley and Hausinger (1989) and Mobley *et al.* (1996)]. In the absence of enzyme, urea is stable in aqueous solutions ranging in pH from 2 to 12, with a half-life of 3.6 years at 38 °C. The nonenzymatic breakdown proceeds via an elimination reaction to release ammonia and cyanic acid (eq 1). In contrast, urease hydrolyzes urea to ammonia and carbamate (eq 2) and the Ni^{2+} ions are thought to act as Lewis acids in catalysis (Zerner, 1991).

(1)

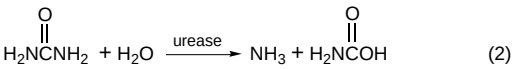

(2)

Synthetic mono- and binickel model compounds have been synthesized to study the nickel requirement of and the role of the nickel center in catalysis. Unfortunately, none of these compounds catalyze the hydrolysis reaction, and it is not clear why nickel, rather than zinc or any other metal ions, is used in urease (Hausinger, 1993). It is known that nickel binds specifically and tightly to urease. Unlike most other metalloenzymes, the removal of the metal ions from urease can only be achieved by harsh treatment with denaturants or acid conditions (Dixon *et al.*, 1980; Zerner, 1991; Martin & Hausinger, 1992). In addition, it has been recently shown that the *in vitro* incorporation of nickel requires carbon dioxide (Park & Hausinger, 1995). *In vivo* the process requires a set of proteins which appear to act as urease-specific chaperones (Moncrief & Hausinger, 1996).

We have recently solved the crystal structure of urease from *Klebsiella aerogenes* (Jabri *et al.*, 1995). The enzyme is a trimer of three T-shaped $\alpha\beta\gamma$ units (Figure 1), each consisting of four structural domains: two in the α-chain and one each in the β- and γ-chains. The α-subunit contains the active site in an $(\alpha\beta)_8$-barrel domain which is homologous to the Zn-dependent enzymes adenosine deaminase (Wilson *et al.*, 1991; Wilson & Quiocho, 1993) and phosphotriesterase (Benning *et al.*, 1995). The two active site nickels are 3.5 Å apart. Ni-1 has an unusual tricoordinate geometry, whereas Ni-2 is pentacoordinate. Finally, a carbamylated lysine, $Lys^{\alpha 217}$*, serves as a bridging ligand for the nickel ions, explaining why carbon dioxide is required for the activation of urease apoenzyme (Park & Hausinger, 1995). Only two other enzymes, ribulose-1,5-bisphosphate carboxylase oxygenase (Rubisco) (Lorimer *et al.*, 1976) and the urease homolog phosphotriesterase (Benning *et al.*, 1995), are known to have carbamylated lysines involved in metal binding. In contrast to urease, however, both Rubisco and phosphotriesterase can be easily inactivated by metal chelators.

[†] This work was supported in part by USDA Grant 9303870 and by NIH Training Grant ST32-GM08384 (to E.J.).

[‡] The coordinates for all structures have been deposited in the Brookhaven Protein Data Bank with access codes 1KRA for the urease apoenzyme, 1KRB for H219A, and 1KRC for H320A.

* To whom correspondence should be addressed.

[§] Current address: Department of Chemistry and Biochemistry, University of Colorado, Boulder, CO 80309-0215.

[⊗] Abstract published in *Advance ACS Abstracts,* August 1, 1996.

S0006-2960(96)00424-2 CCC: $12.00

Table 1: Diffraction Data and Refinement Statistics

data set (no. of crystals)[a]	resolution (Å)	unique reflections (% complete, redundancy)	R_{sym}[b] (%)	protein atoms[c]	solvent atoms	*R*-factor (%)	ideality: bond (Å)	ideality: angles (deg)	resolution (no. of reflections)[d] (Å)
Nat2 (2)	2.2	40 641 (99, 7.9)	10.5	5787	175	17.4	0.008	2.0	10−2.2 (40157)
apoenzyme (2)	2.3	35 214 (98, 7.3)	15.5	5784	179	19.0	0.009	1.9	10−2.3 (34776)
H219A (1)	2.5	27 404 (98, 3.1)	9.5	5782	152	17.9	0.009	1.9	10−2.5 (26626)
H320A (1)	2.5	28 672 (99, 3.3)	9.4	5782	159	18.0	0.008	1.9	10−2.5 (27755)

[a] Crystal sizes were ~470 × 470 × 400 μm for Nat2, ~200 × 200 × 250 μm for apoenzyme, and ~430 × 400 × 360 μm for H219A and H320A mutants. [b] $R_{sym} = \sum|I - \langle I\rangle|/\sum\langle I\rangle$, where I is the integrated intensity of a given reflection from Scalepack. [c] Apoenzyme contains 767 residues and lacks both nickel ions and the CO_2 modification of $Lys^{\alpha 217}$. H219A and H320A contain 767 residues and both nickel ions. [d] Number of reflections used in the refinement.

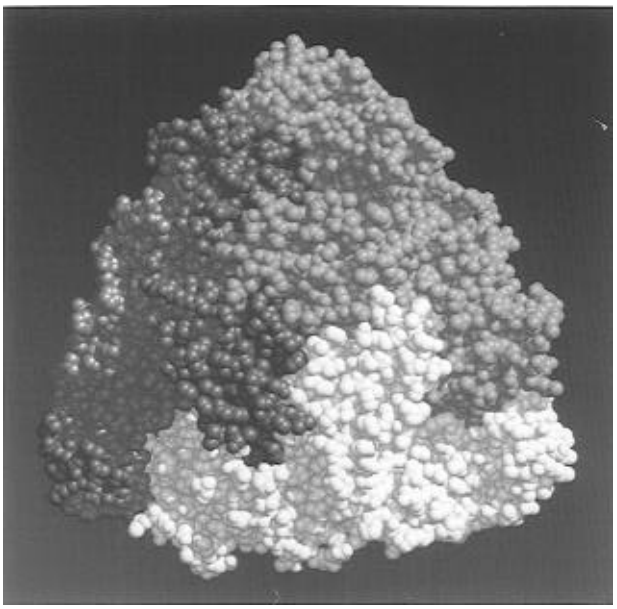

FIGURE 1: Urease structure. Space-filling image showing the tight packing of the urease trimer, with the reference $\alpha\beta\gamma$ unit (yellow), the $\alpha'\beta'\gamma'$ unit (fuschia), and the $\alpha''\beta''\gamma''$ unit (white). The γ-subunits are at the front and center of the trimer. A bit of blue background is visible at the very center because of the cavity existing at the crystallographic 3-fold axis. This figure was prepared with MIDAS (Ferrin, 1988).

Comparisons of small molecule binickel compounds, some which match the Ni−Ni distance (Stemmler *et al.*, 1995) and one with a bound urea (Wages *et al.*, 1993), with the urease metallocenter emphasize that the asymmetric coordination seen in urease and the environment provided by supporting residues make the urease active site unique (Jabri, 1995). Site-directed mutagenesis identified $His^{\alpha 219}$ and $His^{\alpha 320}$ as two residues probably playing key roles in catalysis (Park & Hausinger, 1993a). The $His^{\alpha 219}$ to Ala mutant (H219A) had a K_m of 1100 mM compared to 2.3 mM for wild type with a K_{cat} 3% of the wild type (Park & Hausinger, 1993a). The $His^{\alpha 320}$ to Ala mutant (H320A) showed little change in K_m but had a K_{cat} value of 0.003% of wild type. Furthermore, diethyl pyrocarbonate (DEP)[1] modification of the bacterial urease indicated that a histidine with a pK_a of 6.5 was essential for activity (Park & Hausinger, 1993b) and the residual activity of the H320A mutant was not DEP sensitive (Park & Hausinger, 1993a). These results were interpreted to implicate $His^{\alpha 219}$ in substrate binding and $His^{\alpha 320}$ as the catalytic base.

[1] Abbreviations: F_{apo}, structure factor for apoenzyme; F_{Nat2}, structure factor for native enzyme; HEPES, *N*-(2-hydroxyethyl)piperazine-*N*′-2-ethanesulfonic acid; DEP, diethyl pyrocarbonate.

For accurate interpretation of the properties of site-directed mutants, structural information is very important, as it allows the distinction between direct and indirect effects. Here we probe the tight binding of nickel at the active site and the catalytic mechanism by analysis of the 2.3 Å resolution structure of the apoenzyme and 2.5 Å resolution structures of the two catalytically impaired active site mutants, H219A and H320A.

MATERIALS AND METHODS

Data Collection and Reduction. Details of the purification and crystallization protocol were described previously (Jabri *et al.*, 1992). Crystals grew in hanging drops equilibrated against 100 mM HEPES (pH = 7.5) and 1.6 M Li_2SO_4. All crystals were isomorphous, having cubic space group $I2_13$ with $a = 170.8$ Å, and one $\alpha\beta\gamma$ unit in the asymmetric unit. The holoenzyme structure (at 2.2 Å resolution), designated Nat2 in our original report (Jabri *et al.*, 1995), was our reference structure for phase generation and model building.

Diffraction data for the apoenzyme, H219A, and H320A were collected at room temperature on an ADSC multiwire area detector system as described previously (Jabri *et al.*, 1995) (Table 1). The data were originally processed by the ADSC software, but during preliminary refinement of the apoenzyme, the *B*-factors refined to anomalously low values (near 2 Å^2), suggesting a possible problem with the data. A Wilson plot showed unexpected behavior of the high-resolution data, which rescaling of the data with Scalepack (Otwinowski, 1992) was able to fix (Figure 2). We do not know the cause of the problem, but it appeared to affect the weak, high-resolution data from many of our data sets; thus, data sets Nat2, apoenzyme, H219A, and H320A were all rescaled using Scalepack (Otwinowski, 1992).

The overall R_{sym} of ~15% for the urease apoenzyme data set (Table 1) is high enough to merit special comment. The various analyses of the merging statistics of the data do not suggest that any major systematic difference exists between the two apoenzyme data sets. Figure 3 shows some relevant statistics as a function of resolution to allow a more complete evaluation of data quality. The apoenzyme data set was merged from two crystals, with crystal 1 data having a better overall R_{sym} of 10.7% and crystal 2 having a "terrible" overall R_{sym} of 19.1%. However, a plot of R_{sym} vs resolution reveals that the data from crystal 2 are only slightly worse than those of crystal 1 and that the major difference in overall R_{sym} is due to its sensitivity to how the redundant reflections are distributed (Figure 3a). Furthermore, for the purposes of evaluating reduced data quality, R_{sym} is suboptimal because it reflects the accuracy of individual measurements rather than the accuracy of the reduced data. The main difference

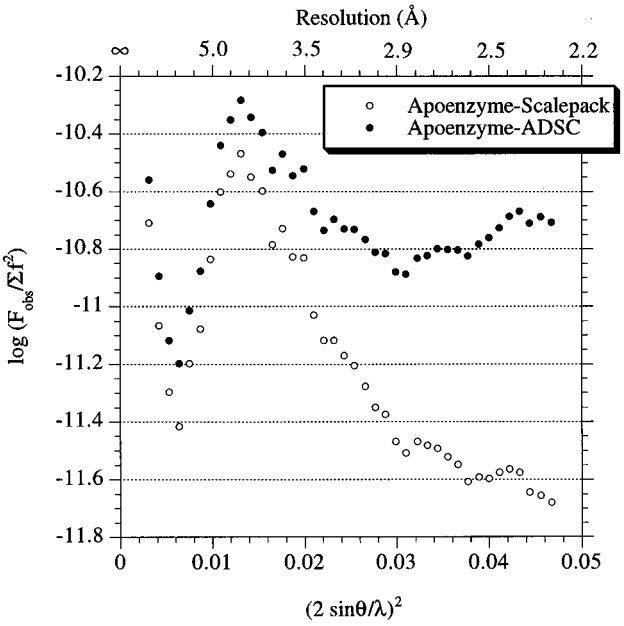

FIGURE 2: Wilson plot of the urease apoenzyme diffraction data processed with the ADSC software (Howard *et al.*, 1985) or with Scalepack (Otwinowski, 1992).

is that increased accuracy obtained through the averaging of many reflections (high redundancy) is not reflected in R_{sym}. An alternate statistic, called R_{int} (for internal *R*-factor), does reflect some of the accuracy gained through high redundancy, because it is calculated from data that have been partially merged (Figure 3). The R_{int} values for the apoenzyme data set (Figure 3b) suggest the data are roughly comparable in quality to other structures we have determined at a similar resolution [e.g., see Figure 2 of Rozwarski *et al.* (1996)]. According to R_{int}, the accuracy of the data sets used in this paper can be ranked Nat2 > Apo > H320A ≈ H219A (data not shown). All four data sets have very high completeness, $\langle I/\sigma \rangle \geq 2.5$, and R_{int} values near or better than 30% at the high-resolution limit reported. Thus, the stated resolution limits accurately reflect the information content of the data sets, and the data sets are all of sufficient quality to support the results we report.

Model Building and Refinement. Further refinement of the native structure against the rereduced Nat2 data yielded an *R*-factor of 17.4% at 2.2 Å resolution (Table 1). The new Nat2 structure is nearly identical to the previously reported model (pdb entry 1KAU), except that all *B*-factors have increased by ∼5 Å^2.

For the apoenzyme structure, electron density maps with coefficients $2F_{apo} - F_{Nat2}$ and $F_{apo} - F_{Nat2}$ and calculated phases were used to assess changes in the structure. On the basis of clear signals, both nickel ions, the CO_2 modification on Lys$^{\alpha 217}$, and two water molecules at the active site were removed from the Nat2 model, and the active site loop (α308−α336) was adjusted. This model was refined for 40 cycles of conjugant gradient minimization and individual *B*-factor refinement against data from 10 to 2.8 Å resolution. After two rounds of manual rebuilding (Sack, 1988) and refinement with X-PLOR (Brünger *et al.*, 1990), higher resolution data (to 2.3 Å) were collected and used in the refinement, resulting in a model with an *R*-factor of 21.2% and an R_{free} of 26.5%. For the final round of refinement, the relative weight for the individual B-factor restraints was set to 0.25 to make it equivalent to that applied to the

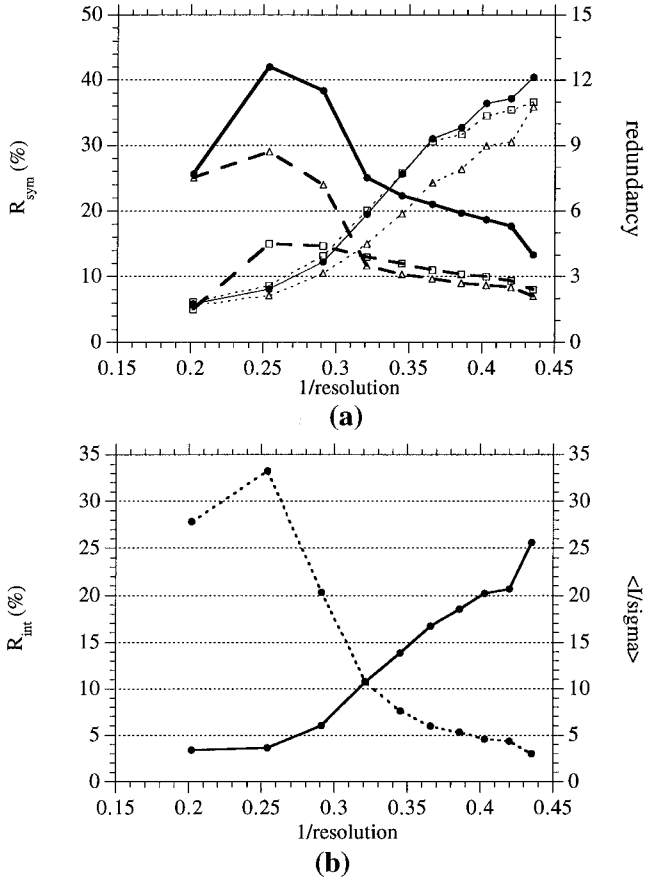

FIGURE 3: Quality assessment of the urease apoenzyme data set. (a) R_{sym} and redundancy are plotted as a function of resolution for crystal 1 (△), crystal 2 (□), and the merged data (●). Crystal 2 was somewhat smaller, and appropriately, the R_{sym} values are slightly higher. The crystal 2 data strategy was designed to maximize the amount of high-resolution data collected. The distibution of redundancy vs resolution is such that the overall R_{sym} of crystal 1 (10.7%) is heavily influenced by the high redundancy of the accurately determined low-resolution reflections, whereas the R_{sym} for crystal 2 (19.1%) is high because it is most heavily influenced by the less accurate high-resolution measurements. This emphasizes that even for data sets of similar quality, the overall R_{sym} can vary over a wide range depending on how the redundancy is distributed. (b) R_{int} and $\langle I/\sigma \rangle$ are plotted as a function of resolution for the merged data set. No absolute standards exist as to what constitutes acceptable data quality, but on the basis of experience, we use cutoffs of R_{int} ∼30% and/or $\langle I/\sigma \rangle$ ∼2 in the high-resolution bin, and this data set is well within those limits. See Table 1 for the definition of R_{sym}. R_{int} is the *R*-factor summed over the Friedel pairs, $R_{int} = 2\Sigma(|F^+ - F^-|)/\Sigma(F^+ + F^-)$, and is calculated from a special data reduction run yielding unmerged Friedel pairs. R_{int} underestimates the final data accuracy because an additional improvement is expected to come from merging the Friedel pairs. $\langle I/\sigma \rangle$ is the average signal-to-noise ratio based on intensities.

holoenzyme structure. The final urease apoenzyme model is at 2.3 Å resolution with 767 residues and 179 solvent molecules and has an *R*-factor of 19.0%. It lacks the two nickel ions as well as the CO_2 modification of Lys$^{\alpha 217}$ (Table 1).

For the H219A mutant, the $F_{H219A} - F_{Nat2}$ map indicated the loss of the His$^{\alpha 219}$ side chain and a movement and ordering of residues α316−α335 in the active site loop. This region of the model was rebuilt, and Wat-1, Wat-170, and the His$^{\alpha 219}$ side chain were removed. A subsequent difference map showed clear density for both water molecules which were then added back. Two more rounds of positional refinement resulted in a model with good geometry with an *R*-factor of 17.9% and R_{free} of 22.3%. Further refinement

using the rescaled H219A data set resulted in a final model with the same *R*-factor (Table 1).

Mutation of $His^{\alpha320}$ to alanine resulted in minor movement of the chain but large shifts in the position of Wat-1 and Wat-170. The model was adjusted accordingly, and Wat-1 and Wat-170 were removed. After refinement, clear density could be seen for Wat-1 bridging the nickel ions, so it was positioned into the density and the model refined to an *R*-factor of 17.4% and with R_{free} of 22.3%. This model was subsequently refined for two more rounds using the rescaled data set and resulted in a final model with an *R*-factor of 18.0% (Table 1).

As with the wild-type enzyme, the metal−ligand distances were not restrained. The geometric parameters of all models have been analyzed using the program PROCHECK (Laskowski *et al.*, 1993). Because of the lower resolution of the analyses for apoenzyme, H219A, and H320A, the isolated movements of buried atoms by ≤0.5 Å are generally not discussed.

Quality of the Models. A Ramachandran plot (Ramachandran & Sasisekharan, 1968) for the holoenzyme and the three new structures shows the same six residues in unusual conformations [note 28 in Jabri et al. (1995)]. The average *B*-value for the holoenzyme is 12.9 $Å^2$ for main chain and 13.5 $Å^2$ for the side chain atoms. The least well ordered region of the model is a loop at the active site (α308−α336). Luzzati plots (Luzzati, 1952) (data not shown) suggest that the coordinate error for the well-ordered portions of the holoenzyme is 0.2 Å, whereas that for the apoenzyme and two active site mutant structures is 0.25 Å. The overall *B*-factors for the apoenzyme and the mutants are comparable to those of the holoenzyme.

Sequence Alignment. Sequence alignments for all ureases were initially generated with the program NCBI TBLASTN (v. 1.4.5MP) (Altschul *et al.*, 1990) using urease from jack bean seed as a query sequence to identify other ureases and related proteins. No other proteins shared significant sequence similarity to urease. Urease sequences were subsequently obtained from NCBI and aligned using the program PileUp in the GCG package (Devereux *et al.*, 1984). The alignment was manually edited where necessary (to remove incorrect gaps) and used for analysis. Secondary structure and solvent accessibility analysis of each residue in urease was completed using the program DSSP (Kabsch & Sander, 1983).

Buried Surface Areas at Interfaces. The solvent-accessible surface area of urease was defined using the algorithm of Richards (1977), as implemented in the program MS (Connolly, 1983). A probe radius of 1.4 Å was used. Surface area buried is defined as $[A_{buried} = (A_s + A_{s'}) - A_{ss'}]$, where S is one subunit, S′ is a second, and SS′ is the S·S′ complex.

RESULTS AND DISCUSSION

Secondary Structure and Residue Conservation. A complete description of the secondary structural elements and an indication of which residues are buried of *K. aerogenes* urease (Jabri *et al.*, 1995) are summarized in Figure 4 along with an alignment of 14 other representative urease sequences. Among the 15 urease sequences, 189 residues (24%) are identical. Although we do not expect that all of these residues will be crucial for catalysis or binding, the conservation pattern of residues is important to take into account when discussing structure−function relations. For clarity, residues will generally be identified by the subunit to which they belong, followed by the residue number (e.g., $Ser^{\alpha2}$ for serine 2 in the α-subunit). Of the conserved residues, six are involved in nickel ligation, and five ($His^{\alpha219}$, $His^{\alpha320}$, $Gly^{\alpha277}$, $Ala^{\alpha363}$, and $Met^{\alpha364}$) are implicated, either by biochemical means or by the structure, in substrate binding or catalysis. In addition, 144 are involved in hydrogen bonding and hydrophobic interactions within one $\alpha\beta\gamma$ unit, and 34 are involved in such interactions to build the $(\alpha\beta\gamma)_3$ trimer (described below).

The Active Site Environment. The nickel-containing active site is located in domain 1 (residues α130−α414) of the α-subunit in the C-terminal portion of the $(\alpha\beta)_8$ barrel. While details of the binickel center have been previously described (Jabri *et al.*, 1995), we present here a somewhat expanded decsription of the active site including the environment of the residues focused on in this study: $Lys^{\alpha217}$* (the CO_2-modified lysine), $His^{\alpha219}$, and $His^{\alpha320}$ (Figure 5).

Both hydrophobic interactions and hydrogen bonds aid in positioning the metal ligands (Figure 5). In particular, $Phe^{\alpha271}$ stacks beneath $His^{\alpha134}$. $His^{\alpha136}$ is positioned through a hydrogen bond from Nδ to the carbonyl of $Thr^{\alpha165}$. The imidazole ring of $His^{\alpha246}$ is packed roughly parallel with that of $His^{\alpha219}$ and forms an additional hydrogen bond with the side chain of conserved residue $Glu^{\alpha220}$. $His^{\alpha272}$ hydrogen bonds to the carbonyl of $Gly^{\alpha278}$ through Nδ1. The carbamate oxygens of the carbamylated lysine, $Lys^{\alpha217}$*, form no secondary hydrogen bonds. However, the Oγ atom of $Thr^{\alpha169}$ is positioned to accept a hydrogen bond from the sp^2 hybridized Nζ atom of $Lys^{\alpha217}$* (Figure 5). $Thr^{\alpha169}$ is conserved in all but the urease from *Lactobacillus fermentum* (Figure 4), where it is an asparagine residue, which could still substitute in this role.

A key catalytic histidine, $His^{\alpha219}$, is buried in the active site and is 3.1 Å from Ni-1 and 3.7 Å from Ni-2. $His^{\alpha219}$ receives a hydrogen bond to Nδ from the main chain nitrogen of $Asp^{\alpha221}$ and therefore exists in a neutral form, protonated on Nϵ. In the Nat2 structure, Nϵ has no hydrogen-bonding partner but points directly at and is 3 Å away from the empty fourth coordination site on Ni-1. Modeling urea into this pocket suggests that Nϵ donates a hydrogen bond to the oxygen of urea and thereby helps position and polarize the substrate.

$His^{\alpha320}$, the putative catalytic base, hydrogen bonds to Wat-170 which in turn hydrogen bonds to Wat-1, a Ni-2 ligand. Since Wat-170 appears to donate hydrogen bonds to two carbonyl oxygens (α363 and α277), $His^{\alpha320}$−Nϵ is probably protonated and donates a hydrogen bond to Wat-170. The pK_a of $His^{\alpha320}$ is influenced by a hydrogen bond to the side chains of $Asp^{\alpha221}$ and the close proximity of $Arg^{\alpha336}$. $His^{\alpha320}$ is positioned such that Nϵ is 4.3 Å away from Wat-1, the putative nucleophilic water molecule, and is then too far away to act as the catalytic base activating Wat-1. Since we do not have a substrate- or inhibitor-bound structure, we cannot dismiss the possibility that a conformational change takes place upon urea binding to position $His^{\alpha320}$ in an appropriate position to act as the catalytic base.

In addition to those within the α-subunit, residues from two loops in a symmetry-related α-subunit (designated α″) position residues at the active site (Figure 5). Specifically $Gly^{\alpha47''}$, in a conserved glycine loop ($Gly^{\alpha46''}$−$Gly^{\alpha48''}$), hydrogen bonds to the carbonyl of $His^{\alpha320}$, and $Phe^{\alpha45''}$ is in van der Waals contact with $Asp^{\alpha221}$. From the second loop,

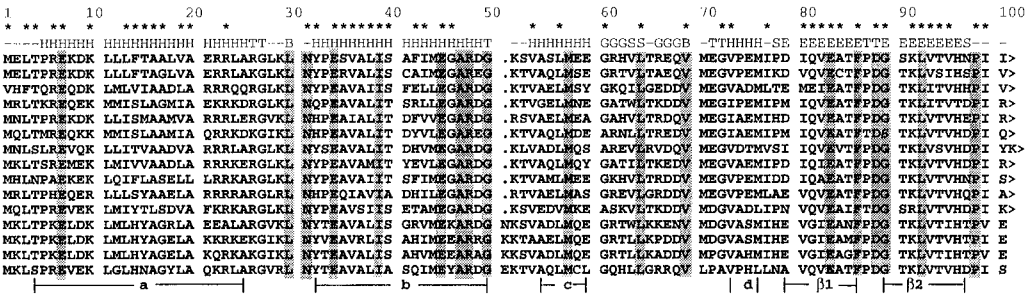

(a)

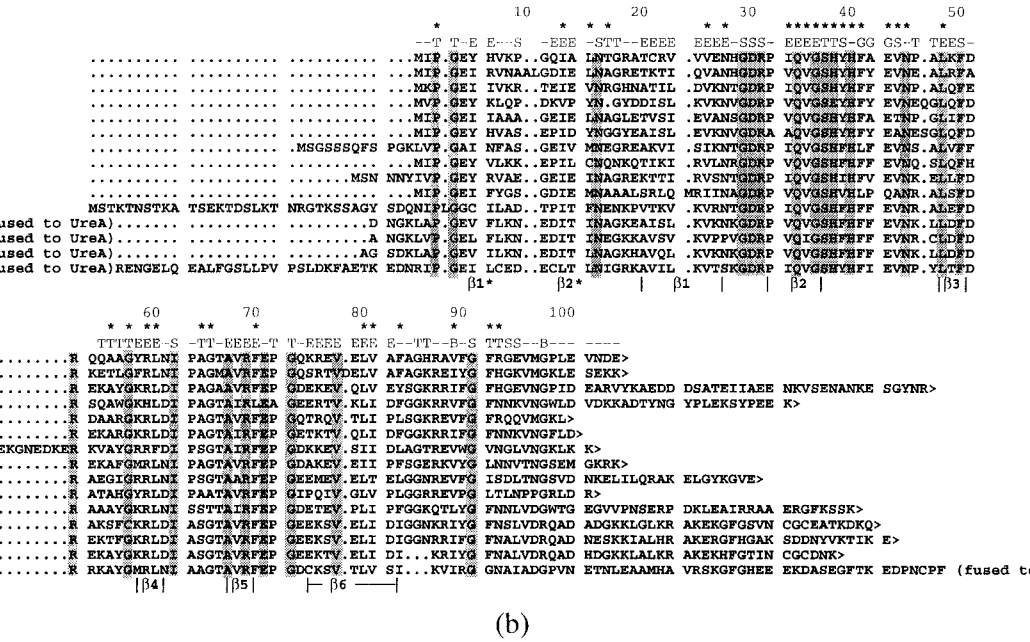

(b)

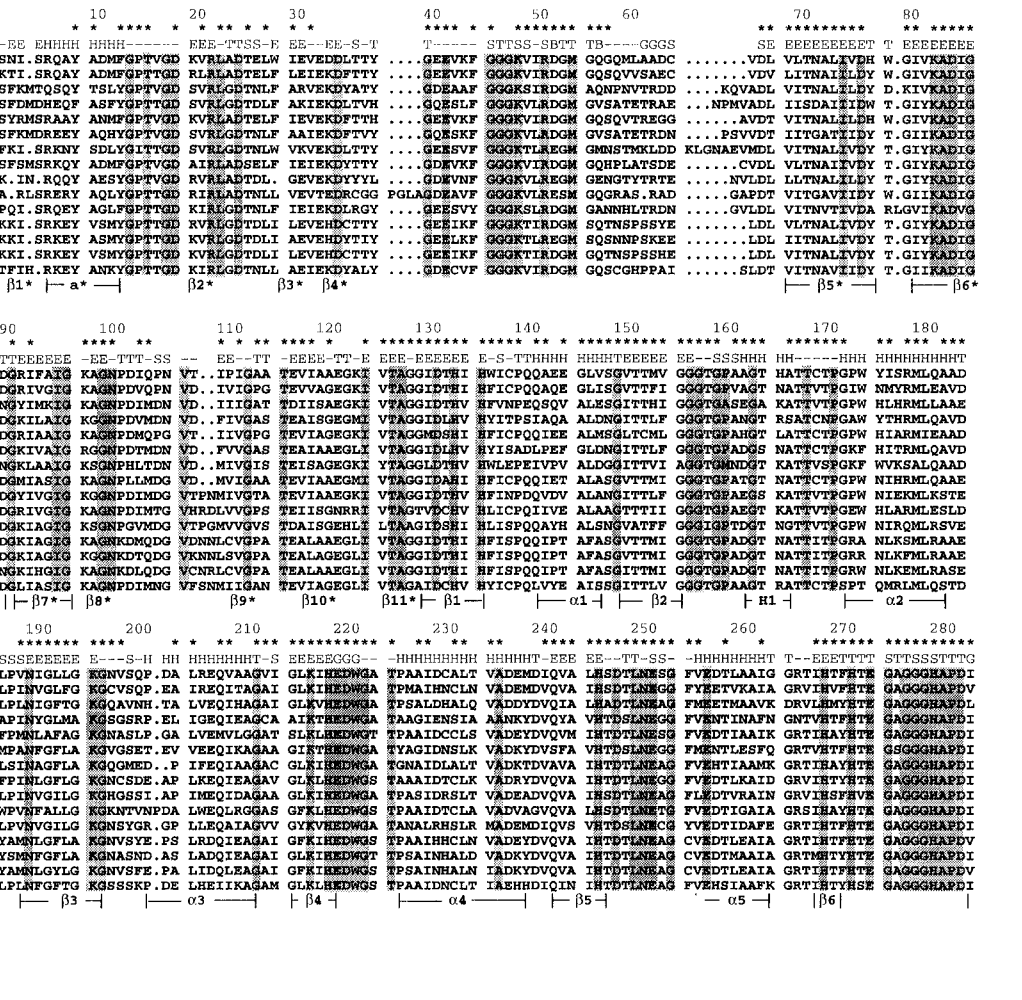

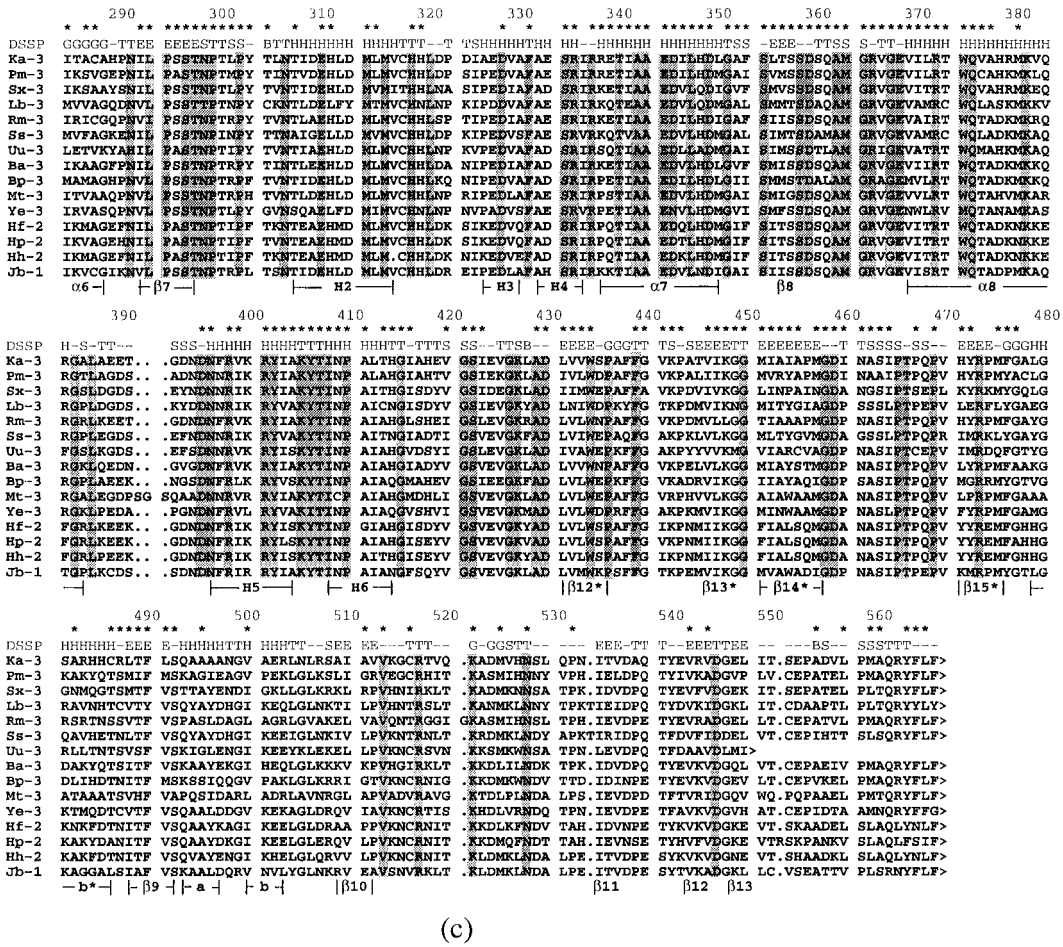

(c)

FIGURE 4: Secondary structure and sequence alignment. Results are shown for the *K. aerogenes* urease (a) γ-subunit, (b) β-subunit, and (c) α-subunit. The residues are numbered according to the *K. aerogenes* sequence (identified residue is under the first digit), with conserved residues highlighted in gray boxes and buried residues (<3% accessibility) marked by an asterisk. DSSP refers to the secondary structure (Kabsch & Sander, 1983) for that residue seen in the 2.2 Å Nat2 structure: H, α helix; E, β strand; T, hydrogen-bonded turn; B, residue in isolated β bridge; G, 3_{10} helix; and S, bend. Nomenclature for the secondary structural elements is given below the sequences. Each sequence is designated by a two-letter abbreviation (below) for the name of the organism from which it was isolated followed by 1, 2, or 3 to indicate the number of chains in that urease. Two-chain ureases have a single chain corresponding to the γ and β chains and one-chain ureases have a single chain corresponding to all three subunits. The C-terminus of each subunit is designated by >, and where appropriate, the fusion of subunits is indicated. Abbreviations used and GenBank accession numbers are as follows: Ka, *Klebsiella aerogenes* (M36068) (Mulrooney & Hausinger, 1990); Pm, *Proteus mirabilis* (M31834) (Jones & Mobley, 1989); Sx, *Staphylococcus xylosus* (X74600) (Jose *et al.*, 1991); Lb, *Lactobacillus fermentum* (D10605) (unpublished); Rm, *Rhizobium meliloti* (S69145) (Miksch *et al.*, 1994); Ss, *Streptococcus salivarius* (U35248) (Chen *et al.*, 1996); Uu, *Ureaplama urealyticum* (L40489) (Neyrolles *et al.*, 1996); Ba, *Bacillus* species thermophilic (D14439) (Maeda *et al.*, 1994); Bp, *Bacillus pastuerii* (X78411) (unpublished); Mt, *Mycobacterium tuberculosis* (U33011) (Reyrat *et al.*, 1995); Ye, *Yersinia enterocolitica* (Z18865) (Skurnik *et al.*, 1993); Hf, *Helicobacter felis* (X69080) (Ferrero & Labigne, 1993); Hp, *Helicobacter pylori* (X17079) (Clayton *et al.*, 1990); Hh, *Helicobacter heilmannii* (L25079) (Solnick *et al.*, 1994); Jb, Jack bean (*Canavalia ensiformis*) (M65260) (Riddles *et al.*, 1992). Other known urease sequences not included here are either >90% identical to a sequence included here or in the case of urease from serotype 7 of *Ureaplasma urealyticum* (Blanchard, 1990) known to have errors.

the carbonyl of Ser$^{\alpha 464''}$ hydrogen bonds to the main chain nitrogen of Met$^{\alpha 364}$. These prominent interactions and more subtle ones link the structure of the active site to the quaternary structure of urease and contribute to durability of the active site toward the loss of nickel ions and mutations.

The Urease Apoenzyme. In order to understand the tight binding of the metal ions in the urease active site, we compared the structure of the urease apoenzyme to that of the holoenzyme. Even in the first $F_{apo} - F_{Nat2}$ difference map, it was clear that the apoenzyme lacked both nickel ions as well as the CO_2 modification of Lys$^{\alpha 217}$. Subsequent refinement at 2.3 Å resolution shows that Wat-173 (*B*-factor of 19.1 Å^2) takes the place of Ni-2 and hydrogen bonds to Nϵ of His$^{\alpha 134}$ (3.0 Å), Nϵ of His$^{\alpha 136}$ (2.9 Å), and Oδ1 of Asp$^{\alpha 360}$ (2.8 Å) (Figure 6). We have modeled Wat-173 as a water because the hydrogen-bonding distances and the electron density match those expected for a water rather than an alternate metal ion. All of the residues which were nickel ligands shift by less than 0.5 Å (Figure 6b) and maintain their secondary interactions.

Overall, the 767 α-carbons overlay with 0.2 Å rms deviation. The only notable structural shifts which occur involve the active site loop (α308−α336), the least well ordered region of the model, which changes its internal structure and becomes more ordered. Specifically, the main chain of residues Phe$^{\alpha 332}$−Ser$^{\alpha 335}$ move up to 2.5 Å such that helices H3 and H4, helical excursions between strand 7 and helix 7 of the $(\alpha\beta)_8$ barrel, merge into a single helix, and the backbone of residues Leu$^{\alpha 311}$−Leu$^{\alpha 316}$, which pack against the altered regions of H3 and H4, shifts by up to 1.5 Å (Figure 7). These changes position Phe$^{\alpha 332}$ deeper into a pocket formed by side chains of residues Glu$^{\alpha 220}$, Asp$^{\alpha 221}$, Thr$^{\alpha 249}$, Leu$^{\alpha 250}$, Leu$^{\alpha 322}$, and Arg$^{\alpha 336}$. The connection between the active site change and the structural changes in the active site loop is not clear. In this regard, we note that whereas helices H2, H3, and H4 move, the loop located in

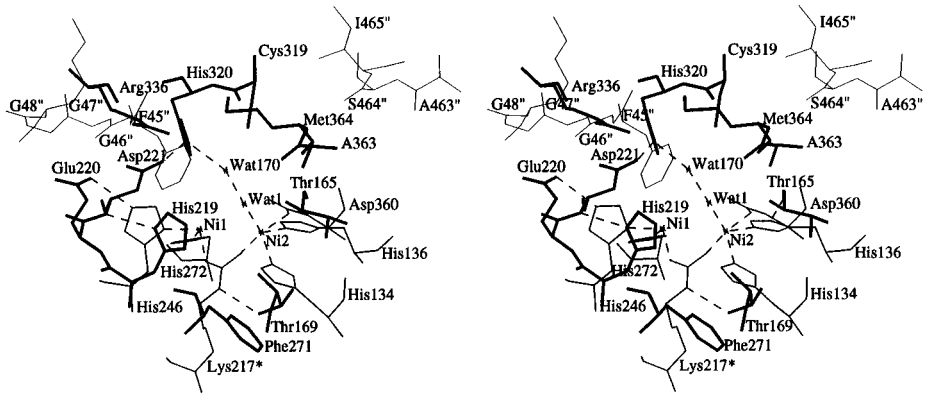

FIGURE 5: Environment of Lys$^{\alpha 217*}$, His$^{\alpha 219}$, and His$^{\alpha 320}$. Metal ligands (medium lines) surrounding residues from the α-subunit (thick lines) and the α″-subunit (thin lines) and some hydrogen bonds (dashed lines) are shown. Thr$^{\alpha 169}$ hydrogen bonds with Nζ of Lys$^{\alpha 217}$*. Glu$^{\alpha 220}$ positions the nickel ligand His$^{\alpha 246}$ through a less commonly observed hydrogen bond involving the *anti* orbital of the carboxylate. His$^{\alpha 219}$ is positioned by a hydrogen bond from the main chain nitrogen of Asp$^{\alpha 221}$ to Nδ. Furthermore, His$^{\alpha 219}$ stacks closely with His$^{\alpha 246}$. Asp$^{\alpha 221}$ and Arg$^{\alpha 336}$ hydrogen bond to His$^{\alpha 320}$. Wat-1 is a ligand to Ni-2 and hydrogen bonds to Wat-170, which in turn hydrogen bonds to His$^{\alpha 320}$. Residues F45″−G48″ and A463″−I465″ from the α″-subunit provide scaffolding for active site residues.

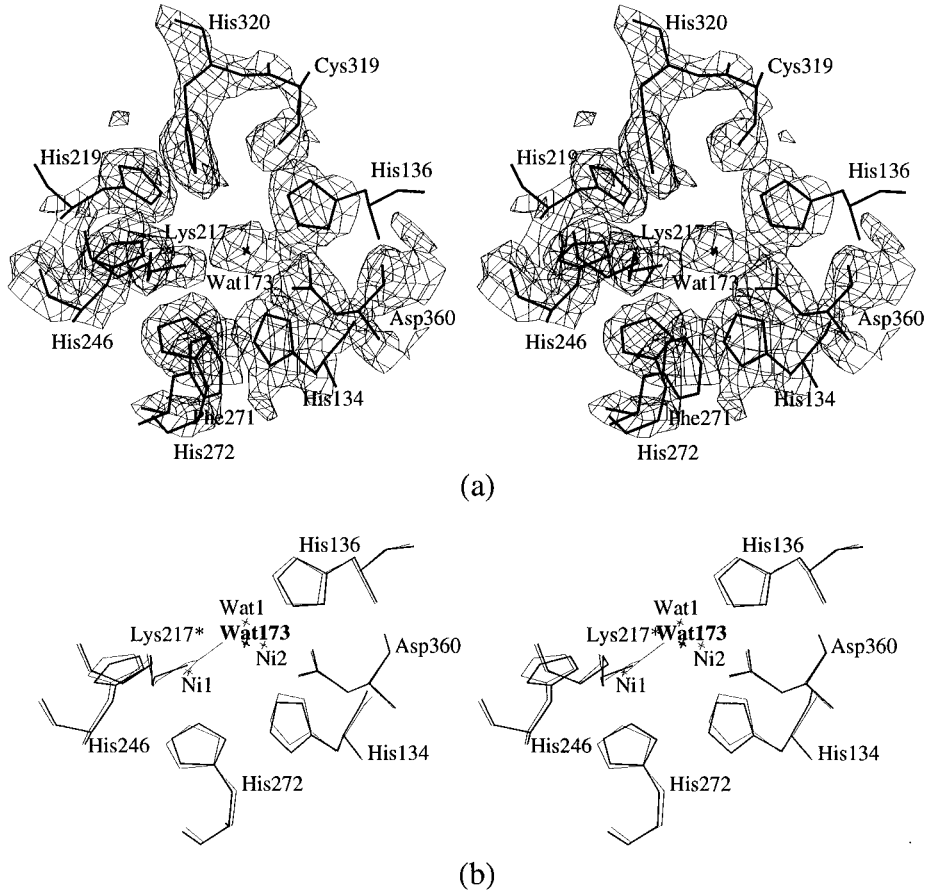

FIGURE 6: Apoenzyme active site. (a) The $2F_o - F_c$ difference electron density contoured at 1.5 times the rms density overlayed on the apoenzyme model clearly shows that the nickel ions and carbamylation of Lys$^{\alpha 217}$ are missing. (b) An overlay of the nickel center of urease holoenzyme (thin lines) and apoenzyme (thick lines) is shown. In the apoenzyme, Wat-173 (bold) takes the place of Ni-2 and forms hydrogen bonds to nickel ligands His$^{\alpha 134}$, His$^{\alpha 136}$, and Asp$^{\alpha 360}$. Otherwise, changes are very small.

between H2 and H3 does not. His$^{\alpha 320}$, the putative catalytic base, is located in this loop and appears to act as a tether for this region of the flap (Figure 7).

Insertion of nickel ions into apoenzyme *in vitro* and *in vivo* requires the carbamylation of Lys$^{\alpha 217}$. *In vivo*, the activation of apoenzyme is thought to be energy dependent, and it has been proposed that efficient insertion of nickel ions into the apoenzyme requires the aid of accessory proteins. It was thought that this might involve a structural change which traps the metal ions in the active site (Moncrief & Hausinger, 1996). Such a structural rearrangement was observed in the enzyme phosphotriesterase, in which binding of the metal ions to the apoenzyme drastically altered the path of the polypeptide chain surrounding the active site (Benning *et al.*, 1995). For the urease apoenzyme, however, the fold appears to fix the nickel binding residues in appropriate positions so that little if any conformational change is associated with nickel binding. This high degree of preorganization probably contributes significantly to the tight binding of nickel.

The H219A Mutant. H219A shows a substantial increase in the K_m in the mutant and a decrease in K_{cat} to 3% of that

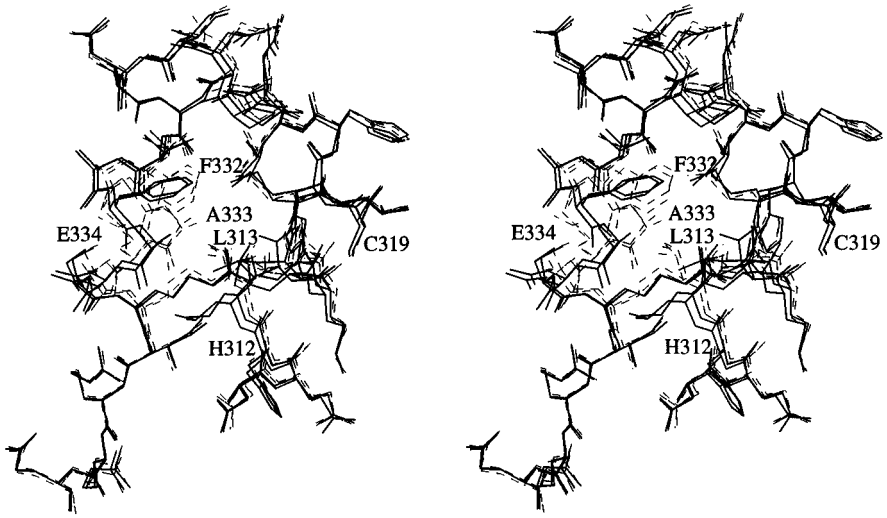

FIGURE 7: Mobility of the active site flap. An overlay of residues α310−α340 of urease holoenzyme (line), apoenzyme (dash), H219A (dash), and H320A (line) shows that the active site flap can adopt various conformations. The holoenzyme and H320A adopt similar conformations. The urease apoenzyme and mutant H219A adopt nearly identical conformations, which are distinct from that of the holoenzyme. In both the apoenzyme and H219A structures, the flap residues are better ordered with *B*-factors ∼20 Å^2 lower than in the other structures.

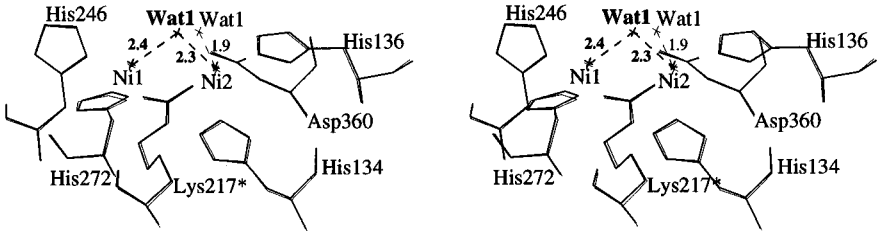

FIGURE 8: Overlay of the holoenzyme (thin lines) with H320A (thick lines) nickel centers. In H320A, Wat-1 (bold), which could also be a hydroxide ion, is 2.4 Å away from Ni-1 and 2.2 Å away from Ni-2. The geometry of Ni-1 is tetrahedral, and that of Ni-2 is distorted square pyramidal with Wat-1 at the apex.

of the wild type (Park & Hausinger, 1993a). These results implicated His$^{\alpha 219}$ in substrate binding, either directly by forming hydrogen bonds to the urea or indirectly by maintaining accessibility to the active site.

Overall, the 2.5 Å resolution structure of the H219A shows only an rms deviation of 0.2 Å from wild type for 767 Cα atoms. Difference maps showed that the major changes are the loss of His$^{\alpha 219}$ and an ordering and movement of the active site flap as had been seen for the apoenzyme (Figure 7). The nickel center and active site residues shift by less than 0.3 Å. Wat-1 and Wat-170 maintain the same position. In wild-type urease, the backbone NH of Asp$^{\alpha 221}$ forms a hydrogen bond to Nδ1 of His$^{\alpha 219}$. In H219A, χ_2 of Asp$^{\alpha 221}$ changes from 5° to 60° so that Oδ2 of Asp$^{\alpha 221}$ replaces Nδ of His$^{\alpha 219}$ in this hydrogen bond. The hydrogen bond between His$^{\alpha 320}$ and Oδ1 of Asp$^{\alpha 221}$ is maintained by a smaller movement of His$^{\alpha 320}$. Given the apparant importance of His$^{\alpha 320}$ to K_{cat}, the small shifts of Asp$^{\alpha 221}$ and His$^{\alpha 320}$ are likely to contribute to the impaired K_{cat} of H219A. However, given that the H320A mutation has little effect on K_m, the large increase in K_m seen for H219A can be confidently assigned to a direct role for His$^{\alpha 219}$ in the binding of urea.

The H320A Mutant. Mutation of His$^{\alpha 320}$ to Ala results in a ∼10^5-fold drop in K_{cat} and a shift in the pH optimum from 7.75 in the wild type to 6.75. These results, as well as DEP modification studies, have implicated this residue as the catalytic base (Park & Hausinger, 1993b). The H320A mutant structure shows an rms deviation of only 0.1 Å from wild type for 767 Cα atoms. Aside from the loss of the His$^{\alpha 320}$ side chain, the only major structural changes are the loss of Wat-170 and a shift of Wat-1, which changes from a Ni-2 ligand to a bridging ligand, positioned 2.4 Å from Ni-1 and 2.3 Å from Ni-2 (Figure 8). The *B*-factor for Wat-1 also drops from 24 to 14 Å^2. In wild-type enzyme, Wat-1 interacts with His$^{\alpha 320}$ via Wat-170 (Figure 5), so it is understandable that Wat-1 is sensitive to this mutation. Because water and hydroxide cannot be distinguished in this analysis, we cannot tell if the structural shift correlates with a change in ionization of Wat-1.

With the shift of Wat-1, the Ni-1 coordination becomes much less unique as it is coordinated by four (two N and two O) ligands in a tetrahedral geometry (Figure 8). Ni-2 maintains its pentacoordinate state, with no significant changes in ligation distances (≤0.25 Å). The ligation angle His$^{\alpha 134}$Nε···Ni-2···Wat-1 decreases by ∼30°, and the angle His$^{\alpha 136}$Nε···Ni-2···Wat-1 increases by ∼30°, so that the geometry at Ni-2 becomes more square pyramidal with Wat-1 at the apex. Other than this, the only notable movement is a 0.4 Å shift of Met$^{\alpha 364}$−Sδ away from the open cavity above the nickel center. Residues Asp$^{\alpha 221}$ and Arg$^{\alpha 336}$, which interact with His$^{\alpha 320}$ in wild type, move by less than 0.5 Å.

As with the H219A mutant, the structure shows that the loss of activity of H320A is not due to a folding defect. However, in contrast to the H219A results, the H320A structure shows a significant structural rearrangement at the metallocenter which could be related to activity loss. If urea does indeed bind at the normally empty fourth coordination site on Ni-1, the filling of this site by Wat-1 in H320A could have major effects on the energetics of catalysis. Thus, in addition to its possible role as a catalytic base, the structure shows that His$^{\alpha 320}$ may have an additional (or alternate) role

in maintaining an active site geometry that allows productive urea binding. These results further emphasize the sensitivity of the nickel coordination to the position of liganding residues like His$^{\alpha 320}$. Ligand-bound structures and additional site-directed mutants of His$^{\alpha 320}$ and its neighbors Asp$^{\alpha 221}$ and Arg$^{\alpha 336}$ should provide additional insight into the role of these residues in the active site.

Trimer of αβγ Units. The structural work reported here and the original mutagenesis work (Park & Hausinger, 1993a) show that the conformation and stability of the enzyme are remarkably insensitive to loss of nickel ions and active site mutations. Although extensive stability studies have not been done on *K. aerogenes* urease, the closely related jack bean urease (Figure 4) shows remarkable resistance to denaturation: 50% of its activity remains after treatment with 2 M guanidinium chloride, pH 7.6, and 2.5 μM EDTA at 38 °C for 2 h, and 25% remains after treatment with 9 M urea, pH 9, at 25 °C for 24 h (Dixon *et al.*, 1980). In light of these results, we describe here the extensive quaternary interactions which contribute to this remarkable stability.

Urease is a tightly associated trimer of three $\alpha\beta\gamma$ units located around a crystallographic 3-fold axis (Figure 1). These units are described by the symmetry operators *xyz*, *zxy*, and *yzx* and will be referred to as $\alpha\beta\gamma$, $\alpha'\beta'\gamma'$, and $\alpha''\beta''\gamma''$, respectively. Each $\alpha\beta\gamma$ unit makes extensive contacts to build the trimer: the α-subunit (in addition to interactions with β- and γ-subunits) packs between α′ and α″ and also contacts β'' and γ'', the β-subunit packs with α′ (equivalent to the α·β'' interaction), and the γ-subunit interacts with α′ (equivalent to the α·γ'' interaction) and with γ' and γ'' at the 3-fold axis. The packing involves numerous hydrogen bonds and hydrophobic interactions between $\alpha\beta\gamma$ units.

Approximately 6130 Å^2 (23%) surface of each $\alpha\beta\gamma$ unit (~18 400 Å^2 total for the trimer) is buried upon trimer formation so that in all a remarkable 55% of the residues in the $\alpha\beta\gamma$ unit are buried (<3% accessible): 50/100 in the γ-subunit, 32/106 in the β-subunit, and 342/566 in the α-subunit. These buried residues include 150 (77%) of the conserved residues. In the α-subunit there is even one stretch with 37/38 residues (α341−α378) buried (Figure 4). The specific residues making 64 unique (192 total) hydrogen bonds at the interfaces of the trimer and the surface areas buried in these contacts are given in Tables 2 and 3, respectively.

Specifically, the α-subunits pack in a head-to-tail arrangement with domain 2 of α contacting domain 1 of α′. The main contacts involve residues in strand 7, helix H1, and loops 3, 4, 5, 6, and 8 of the $(\alpha\beta)_8$ barrel interacting with the loops after strands 4, 9, and 14 in domain 2 of the α′-subunit. The interactions between α and α″ are simply the reverse of the α·α′ interactions. Two segments from the α″-subunit (Phe$^{\alpha 45''}$−Gly$^{\alpha 48''}$ and Ala$^{\alpha 463''}$−Ile$^{\alpha 465''}$) make contact with the active site residues (Figure 5), providing a link between quaternary structure and catalytic activity. The interactions of α with β'' are primarily between loop 5 in the $(\alpha\beta)_8$ barrel and strand 2 and the following irregular loop of the β''-subunit. The N-terminus of γ'' interacts with strand 15 in domain 2 of the α-subunit. Also, residues in strands 1 and 2 at the C-terminus of γ'' interact with residues in helical excursion H2 and helix 8 of the $(\alpha\beta)_8$ barrel as well as the C-terminal tail of α. Both the γ''- and β''-subunits provide a scaffold for residues from the active site flap (α308−α336). Although few hydrogen bonds are involved in these interactions, residues β68″−β70″ pack against

Table 2: Intersubunit Hydrogen Bonds in the Urease Trimer[a]

α	β	α	γ
Ser2−O	Leu15−N	*Asp460−Oδ2	Lys10−Nζ
Ser2−N	Asn62−Oδ1	Ser464−N	*Glu83−Oε1
Ile4−N	Ile13−O	Ser464−Og1	*Glu83−Oε1
Ile4−O	Ile13−N	*Thr467−Oγ1	Gln81−Nε2
*Asp19−Oδ1	Lys9−N	Gln469−N	Gln81−O
Lys20−N	His7−O	His472−Nε2	Asp9−Oδ2
Lys20−O	His7−N	*Arg474−Nη1	Asp9−Oδ1
*Arg22−N	Glu5−O	*Arg474−Nη2	Asp9−Oδ1
*Arg22−Nη1	Glu5−Oε1	Gln562−O	*Asn31−Nδ2
*Arg22−Nη2	Glu5−Oε2	Arg563−Nε	Glu71−O
Ala24−O	Gly4−N	Arg563−O	Tyr32−N
Tyr39−O	*Asn16−N	Phe565−O	*Asn31−Nδ2
Glu41−Oε2	Arg19−Nη1	Leu566−O	Arg23−Nη2
Glu41−Oε2	Arg19−Nη2		
Glu41−Oε1	His39−Nε		
Glu41−Oε2	Arg60−Nη1		
Pro102−O	His87−N		
Asp103−O	His87−N		
Asp103−Oδ1	His87−Nδ		
Asp103−O	Arg88−N		
Asp103−O	Ala89−N		
Ile104−O	Ala85−N		

α	α′	α	β″
*Lys49−Nζ	*Asp329−Oδ2	Ala227−N	Phe93−O
*Arg52−Nη1	*Glu252−Oε1	*Leu250−O	*Gln35−N
*Arg52−Nη2	*Glu252−Oε2	*Asn251−Nδ2	Pro33−O
Asp53−N	*Trp222−O	*Asn251−O	*Asn46−Nδ2
Asp53−Oδ2	Ser200−Oγ1	*Glu252−O	*Asn46−N
Gln57−Oε1	*Lys196−Nζ	*Glu252−Oε2	*Gly37−N
Ala62−N	Glu207−Oε2	Ser253−O	Arg94−Nη2
*Gly113−O	*Lys196−Nζ	*Glu257−Oε2	*Arg32−Nη1
*Thr116−O	*Lys196−Nζ	*Glu257−Oε1	*Arg32−Nη2
Glu117−Oε1	Thr159−Oγ1	*Asp283−Oδ1	*Arg32−N
Glu117−Oε1	Thr165−Oγ1	Glu328−O	*Gln35−Nε2
Val118−O	*Gly164−N		
*Gly451−O	Trp176−OH		
Asn462−Oδ2	*Gly369−N		
Ser464−O	*Met364−N		
Pro475−O	Gln141−Nε2		

γ	γ′	α	γ″
Glu2−Oε1	Tyr32−OH	Glu145−Oε2	Arg6−Nη2
Glu21−Oε1	Arg22−Nη2	Glu145−Oε2	Arg6−N
Glu21−Oε2	Arg22−Nη1	Thr305−Oγ1	Lys91−Nζ
*Glu45−Oε1	Arg23−Nε	Thr305−Oγ1	*Asp88−Oδ1
*Glu45−Oε2	Arg23−Nη1	*Asn307−N	*Asp88−Oδ1
*Glu45−Oε1	Arg26−Nη2	*Asn307−Nδ2	*Asp88−Oδ1
*Glu45−Oε2	Arg26−Nη2	*Asn307−Nδ2	*Asp88−Oδ2
*Glu45−Oε1	Arg26−Nη1	*Asn307−Oδ1	Val53−N
*Arg48−Nε	Lys29−O	*Glu311−Oε1	*Leu92−N
*Arg48−Nε	*Glu34−Oε1	*Arg366−Nε	*Glu83−Oε2
*Arg48−Nη2	*Glu34−Oε1	*Arg366−Nη2	*Glu83−Oε1
Asp49−Oδ1	Arg26−Nε	*Glu369−Oε1	Ser90−Oγ1
Asp49−Oδ1	Arg26−Nη2	*Arg373−Nη2	Ser90−O
		Lys443−Nζ	*Glu7−Oε1
		Lys443−Nζ	Met1−O
		Val471−O	Glu2−N
		Val471−O	Leu3−N
		His472−Nδ	Lys8−Nζ
		Tyr473−N	Leu3−O
		Leu558−N	Pro87−O
		Gln562−Nε2	*Ala47−O
		Gln562−Nε2	Thr85−O
		Leu566−N	Glu7−Oε1
		Phe567−O	Thr85−N

[a] Hydrogen bonds were identified using HBPlus (McDonald *et al.*, 1993). Conserved residues are denoted with an asterisk (*). Interactions within the $\alpha\beta\gamma$ unit are shown in the top two columns and interactions between symmetry-related $\alpha\beta\gamma$ units are shown in the bottom four columns. Note that each interaction listed here occurs three times in the $(\alpha\beta\gamma)_3$ trimer.

Table 3: Buried Surface Areas at the Subunit−Subunit Interfaces

interfaces involving α, α′, α″		interfaces involving β, β′, β″		interfaces involving γ, γ′, γ″	
αα	NA	αβ	2180 (8.5)	αγ	1030 (4.1)
αα′	2930 (7.0)	αβ′	0 (0.0)	αγ′	0 (0.0)
αα″	2940 (7.0)	αβ″	960 (3.7)	αγ″	1620 (6.3)
βα	2180 (8.5)	ββ	NA	βγ	110 (1.0)
βα′	950 (3.7)	ββ′	0 (0.0)	βγ′	0 (0.0)
βα″	0 (0.0)	ββ″	0 (0.0)	βγ″	0 (0.0)
γα	1030 (4.1)	γβ	110 (1.0)	γγ	NA
γα′	1630 (6.4)	γβ′	0 (0.0)	γγ′	630 (5.7)
γα″	0 (0.0)	γβ″	0 (0.0)	γγ″	620 (5.7)

[a] Areas are given in Å^2 followed by the percentage buried [$=A_{buried}/(A_s + A_{s'}) \times 100$] in parentheses. Surface areas were calculated using MS (Connolly, 1983). NA, not applicable.

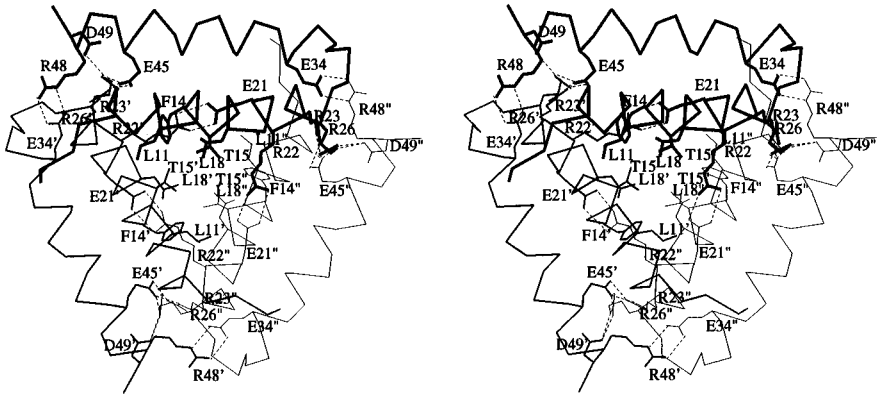

FIGURE 9: Interactions of the γ-subunits around the 3-fold axis. Residues from helices a and b in the γ-subunit (L11, F14, T15, L18, E21, R22, R23, E34, E45, R48, and D49) are involved in interactions with residues in helices a and b of the γ′- and γ″-subunits. These helices pack around the crystallographic 3-fold and facilitate the interaction of symmetry-related αβγ units. Some hydrogen bonds (≤3.4 Å) are shown as dashed lines.

residues α328−α332, and residues γ86″−γ92″ pack against residues α307−α316.

The packing of γ-subunits at the crystallographic 3-fold axis is dominated by three copies of helix a, one each from γ, γ′, and γ″, which pack against one another in an almost orthogonal manner (Figure 9). A series of hydrophobic residues including Leu$^{\gamma 11}$, Phe$^{\gamma 14}$, Leu$^{\gamma 18}$, and Val$^{\gamma 19}$ and their symmetry mates provide a core for the helix-packing interactions. Also, three acidic residues on helices a and b of γ make extensive interactions with three Arg residues on helix **a** of γ′ (Table 2, Figure 9).

Although the γ-subunits pack closely on the 3-fold axis, the α-subunits do not, so a large elliptical cavity exists which extends 35 Å along the 3-fold axis and has an ∼15 Å diameter at its widest point. The pocket is separated from solvent on one side by three symmetry-related γ-subunits and on the other side by the side chains of Arg$^{\alpha 508}$ and its symmetry mates. Side chains from residues Ile$^{\alpha 138}$−Ser$^{\alpha 149}$, Ala$^{\alpha 183}$−Pro$^{\alpha 188}$, Met$^{\alpha 452}$−His$^{\alpha 485}$, Asn$^{\alpha 506}$−Ser$^{\alpha 509}$, and Met$^{\gamma 1}$−Leu$^{\gamma 24}$ from all three symmetry-related αβγ units line the pocket. Bulk solvent fills this cavity, and some uninterpretable peaks of higher density may represent partially localized buffer molecules (sulfate, HEPES).

Recently, Chan and colleagues (Chan *et al.*, 1995) suggested that the stability of the hyperthermophilic enzyme aldehyde ferredoxin oxidoreductase (AOR) may be related to its uniquely low surface to volume ratio, as it had only 85% of the surface area expected for a protein of its size and 55% of its atoms were completely buried. Both of these numbers were more extreme than any in a reference set of 30 monomeric and oligomeric proteins (∼300 to ∼2400 residues). Using the definitions of Chan and colleagues (Chan *et al.*, 1995), urease has only 81% of the surface area expected for a protein of its size and buries (zero accessible surface area) 59% of its atoms, making the urease values even more extreme than those of AOR! Although *K. aerogenes* urease does have a relatively high thermal transition, near 80° (Lee *et al.*, 1990), it loses activity upon prolonged incubations at 55° (Park & Hausinger, 1993a), showing it has lower stability than enzymes from hyperthermophiles. These observations are consistent with the extensive core of urease being a major factor in its stability, but they also emphasize that there must be other factors contributing to hyperthermostability which are not present in urease.

ACKNOWLEDGMENT

We thank Robert P. Hausinger and members of his laboratory for providing wild-type and mutant *K. aerogenes* urease and for many fruitful discussions. We also thank Barbara Golden, Andrew Feig, and Phil Hammond for critical reading of the manuscript and helpful discussion. We thank the referees for noting the importance of further documenting the quality of the apoenzyme data set.

REFERENCES

Altschul, S. F., Gish, W., Miller, W., Myers, E., & Lipman, D. J. (1990) *J. Mol. Biol. 215*, 403−410.

Benning, M. M., Kuo, J. M., Raushel, F. M., & Holden, H. M. (1995) *Biochemistry 34*, 7973−7978.

Blanchard, A. (1990) *Mol. Microbiol. 4*, 669−676.

Brünger, A. T., Krukowski, A., & Erickson, J. W. (1990) *Acta Crystallogr. A46*, 585−593.

Chan, M. K., Muklund, S., Kletzin, A., Adams, M. W. W., & Rees, D. C. (1995) *Science 267*, 1463−1469.
Chen, Y. Y., Clancy, K. A., & Burne, R. A. (1996) *Infect. Immun. 64*, 585−592.
Clayton, C. L., Pallen, M., Kleanthous, H., Wren, B. W., & Tabaqchali, S. (1990) *Nucleic Acids Res. 18*, 362.
Connolly, M. L. (1983) *Science 221*, 709−713.
Devereux, J., Haiberli, P., & Smithies, O. (1984) *Nucleic Acids Res. 12*, 387−395.
Dixon, N. E., Gazzola, C., Asher, C. J., Lee, D. S., Blakeley, R. L., & Zerner, B. (1980) *Can. J. Biochem. 58*, 474−480.
Ferrero, R. L., & Labigne, A. (1993) *Mol. Microbiol. 9*, 323−333.
Ferrin, T. E. (1988) *J. Mol. Graphics 6*, 13−27.
Hausinger, R. P. (1993) in *Biochemistry of Nickel*, pp 23−50, Plenum Press, New York.
Howard, A. J., Nielson, C., & Xuong, N. H. (1985) *Methods Enzymol. 114*, 452−472.
Jabri, E. (1995) Crystal structure of the holo-, apo-, and three active site mutants of urease from *Klebsiella aerogenes*, Ph.D. Thesis, Cornell University, Ithaca, NY.
Jabri, E., Lee, M. H., Hausinger, R. P., & Karplus, P. A. (1992) *J. Mol. Biol. 227*, 934−937.
Jabri, E., Carr, M. B., Hausinger, R. P., & Karplus, P. A. (1995) *Science 268*, 998−1004.
Jones, B. D., & Mobley, H. L. T. (1989) *J. Bacteriol. 171*, 6414−6422.
Jose, J., Christians, S., Rosenstein, R., Götz, F., & Kaltwasser, H. (1991) *FEMS Microbiol. Lett. 80*, 277−282.
Kabsch, W., & Sander, C. (1983) *Biopolymers 22*, 2577−2637.
Laskowski, R. A., MacArthur, M. W., Moss, D. S., & Thornton, J. M. (1993) *J. Appl. Crystallogr. 26*, 283−291.
Lee, M. H., Mulrooney, S. B., & Hausinger, R. P. (1990) *J. Bacteriol. 172*, 4427−4431.
Lorimer, G. H., Badger, M. R., & Andrews, T. J. (1976) *Biochemistry 15*, 529−536.
Luzzati, P. V. (1952) *Acta Crystallogr. 5*, 802−810.
Maeda, M., Hidaka, M., Nakamura, A., Masaki, H., & Uozumi, T. (1994) *J. Bacteriol. 176*, 432−442.
Martin, P. R., & Hausinger, R. P. (1992) *J. Biol. Chem. 267*, 20024−20027.
McDonald, I. K., Naylor, D. N., Jones, D. T., & Thornton, J. M. (1993) *HBPlus*, Department of Biochemistry and Molecular Biology, University College, London.
Miksch, G., Arnold, W., Lentzsch, P., Priefer, U. B., & Puhler, A. (1994) *Mol. Gen. Genet. 242*, 539−550.
Mobley, H. L. T., & Hausinger, R. P. (1989) *Microbiol. Rev. 53*, 85−108.
Mobley, H. L. T., Island, M. D., & Hausinger, R. P. (1996) *Microbiol. Rev.* (in press).
Moncrief, M. C., & Hausinger, R. P. (1996) in *Mechanisms of Metallocenter Assembly* (Hausinger, R. P., Eichhorn, G. L., & Marzilli, L. G., Eds.) pp 151−171, Elsevier Press, New York.
Mulrooney, S. B., & Hausinger, R. P. (1990) *J. Bacteriol. 172*, 5837−5843.
Neyrolles, O., Ferris, S., Behbahani, N., Montagnier, L., & Blanchard, A. (1996) *J. Bacteriol. 178*, 647−655.
Otwinowski, Z. (1993) in *Data Collection and Processing* (Sawyer, L., Isaacs, N., & Bailey, S. S., Eds.) pp 55−62, SERC Daresbury Laboratory, Warrington, U.K.
Park, I.-S., & Hausinger, R. P. (1993a) *Protein Sci. 2*, 1034−1041.
Park, I.-S., & Hausinger, R. P. (1993b) *J. Protein Chem. 12*, 51−56.
Park, I.-S., & Hausinger, R. P. (1995) *Science 267*, 1156−1158.
Ramachandran, G. N., & Sasisekharan, V. (1968) *Adv. Protein Chem. 23*, 283−427.
Reyrat, J. M., Berthet, F. X., & Gicquel, B. (1995) *Proc. Natl. Acad. Sci. U.S.A. 92*, 8768−8772.
Richards, F. M. (1977) *Annu. Rev. Biophys. Bioeng. 6*, 151−176.
Riddles, P. W., Whan, V., Blakeley, R. L., & Zerner, B. (1992) *Gene (Amsterdam) 108*, 265−268.
Rozwarski, D. A., Diederichs, K., Hecht, R., Boone, T., & Karplus, P. A. (1996) *Proteins: Struct., Funct., Genet.* (in press).
Sack, J. S. (1988) *J. Mol. Graphics 6*, 224−225.
Skurnik, M., Batsford, S., Mertz, A., Schiltz, E., & Toivanen, P. (1993) *Infect. Immun. 61*, 2498−2504.
Solnick, J. V., O'Rourke, J., Lee, A., & Tompkins, L. S. (1994) *Infect. Immun. 92*, 1631−1638.
Stemmler, A. J., Kampf, J. W., Kirk, M. L., & Pecoraro, V. L. (1995) *J. Am. Chem. Soc. 117*, 6368−6369.
Wages, H. E., Taft, K. L., & Lippard, S. J. (1993) *Inorg. Chem. 32*, 4985−4987.
Wilson, D. K., & Quiocho, F. A. (1993) *Biochemistry 32*, 1689−1694.
Wilson, D. K., Rudolph, F. B., & Quiocho, F. A. (1991) *Science 252*, 1278−1284.
Zerner, B. (1991) *Bioorg. Chem. 19*, 116−131.

BI960424Z